Annales Societatis Geologorum Poloniae (2020), vol. 90: 447–462 doi: https://doi.org/10.14241/asgp.2020.19

MAASTRICHTIAN CLIMATE CHANGES – THE CALCAREOUS NANNOFOSSIL RECORD FROM FLYSCH DEPOSITS OF THE OUTER CARPATHIANS

Adam WIERZBICKI* & Mariusz KĘDZIERSKI

Jagiellonian University, Faculty of Geography and Geology, Institute of Geological Sciences, Gronostajowa 3a, Kraków, Poland; e-mails: adam.wierzbicki@doctoral.uj.edu.pl; mariusz.kedzierski@uj.edu.pl
** Corresponding author*

Wierzbicki, A. & Kędzierski, M., 2020. Maastrichtian climate changes – the calcareous nannofossil record from flysch deposits of the Outer Carpathians. *Annales Societatis Geologorum Poloniae,* 90: 447–462.

Abstract: The Outer Carpathians are known for a few sections, where transitions from the Upper Cretaceous to the Palaeogene, including the K-Pg boundary interval, were described. One of them, the Bąkowiec section in the Skole Nappe, was examined with reference to the record of biostratigraphy and palaeoenvironmental changes, mainly based on the analysis of calcareous nannofossil assemblages. This study shows no evidence for the K-Pg boundary; however, the presence of the nannofossil species *Micula prinsii*, marking the topmost Maastrichtian UC20d^{TP} Zone, was noted. The appearance of this low-latitude taxon and relevant changes in the composition of nannofossil assemblages indicate an influx of Tethyan warm water into the northern Carpathian basins during the latest Maastrichtian, shortly before the K-Pg boundary event. Therefore, the authors infer that the upper part of the Bąkowiec section recorded the latest Maastrichtian warming of climate, probably triggered by Deccan volcanic activity.

Key words: Late Maastrichtian warming, Deccan traps, K-Pg boundary, biostratigraphy, Skole Nappe.

Manuscript received 05 August 2020, accepted 20 October 2020

INTRODUCTION

The Maastrichtian, last of the Cretaceous stage, was ended by Cretaceous/Palaeogene (K-Pg) extinction event, recognized as one of the five most severe extinctions throughout the entire Phanerozoic. Therefore, this event marks also beginning of a new era (the Cenozoic). Naturally, such a phenomenon focused the attention of many scientists, leading over time to the enunciation of two main hypotheses explaining possible causes of the event, i.e. an asteroid impact (Alvarez *et al*., 1980) or intense volcanism (MacLean, 1985).

However, these two possible circumstances, which could have led to the end-Cretaceous catastrophe, differ basically in the time of duration, i.e. the rapidness of change, and the stratigraphic position of their record. Thus, the evidence of a sudden and very short-lived extraterrestrial bolide impact ending the Maastrichtian would have been recorded in post-impact deposits belonging stratigraphically to the youngest Danian, or the Cenozoic. In contrast, volcanism during some period before the extinction event should have left its footprint below the K-Pg boundary.

Indeed, many studies of the uppermost Maastrichtian deposits revealed their individual geochemical feature that may be linked to phase 2 of Deccan volcanism, initiated ca. 250 kyr before the end of Cretaceous (e.g., Abrajevitch *et al.,* 2015; Punekar *et al.,* 2016; Sprain *et al.,* 2019). The geochemical studies have been supplemented by the palaeontological record predating directly the K-Pg extinction event and indicating pronounced changes in, for instance, foraminiferal assemblages (e.g., Tantawy *et al*., 2009; Dubicka and Peryt, 2012; Keller *et al*., 2016; Dameron *et al*., 2017; Mateo *et al*., 2017), ammonites (e.g., Marshall and Ward, 1996) or nannofossils (e.g., Sheldon *et al*., 2010; Thibault and Husson, 2016).

However, the environmental changes, recorded in a global scale, also affected other marine or terrestrial biota throughout the entire Maastrichtian (e.g., Hallam and Perch-Nielsen, 1990; Barrera and Savin, 1999; Li and Keller, 1999; Nordt *et al.,* 2003). For example, the dinosaurs, iconic Mesozoic animals, gradually became extinct, starting at least 7 Myr before K-Pg boundary (Sloan *et al*., 1986; Brusatte *et al.,* 2015; Sakamoto *et al*., 2016).

Other changes on land were marked by angiosperm radiation in the Cretaceous. While the angiosperm onset is dated as mid-Cretaceous (Davis *et al*., 2005) they became the most species-rich group among other plant clades during the Maastrichtian (Wing and Boucher, 1998; Peralta-Medina

and Falcon-Lang, 2012). This angiosperm radiation, followed by their predominance, probably influenced the frequency and severity of surface wildfires, because the angiosperms fuelled more ecologically harmful fires (Belcher and Hudspith, 2017). Furthermore, the disappearance of the inoceramids, one of the most interesting bio-events preceding the K-Pg boundary event, happened around the early/late Maastrichtian transition (the so-called mid-Maastrichtian Event, MME; see Voigt *et al.,* 2012). This extinction is also attributed to the Maastrichtian environment (climate) changes (e.g., MacLeod, 1994; Elorza and García-Garmilla, 1998; Gómez-Alday *et al*., 2004). In addition, six ammonite extinctions occurred throughout the Late Cretaceous, mostly during the Maastrichtian (Marshall and Ward, 1996).

Altogether, the Maastrichtian environmental changes may be visualised as climate changes that ended the Cretaceous warm greenhouse or, at times, hothouse conditions, and gradually transformed into a cold greenhouse climate mode (e.g., Linnert *et al.,* 2014). Accordingly, the Maastrichtian is generally considered to have been much colder than the rest of the Cretaceous ages and possibly even the coolest (e.g., Huber *et al*., 2018). Naturally, the question arises: what drove this climate cooling? One of the main factors evoked here is the reorganization of deep ocean circulation by Atlantic cold, high-latitude, deep or intermediate water masses (MacLeod and Huber, 1996; MacLeod *et al.,* 2011; Donnadieu *et al*., 2016) that resulted in a long-term climate switch. Meaningfully, the cooling was accompanied by, or followed, Late Cretaceous tectonic events, such as mid-Maastrichtian Laramide tectonism or subsidence of the Rio Grande Rise-Walvis Ridge (Frank and Arthur, 1999), also reorganizing the northern Tethys margin (e.g., Masse *et al*., 1995), as well as, low rate of ocean crust production resulting in the long-term fall of sea level (Larson, 1991). Diastrophism and a fall in sea level enhanced chemical weathering and gave rise to a subsequent decrease in the level of atmospheric CO_2 (Gale, 2011). The Maastrichtian lowstand resulted in a reduction in the area occupied by epicratonic and marginal seas and triggered the re-appearance of shelf-break and caballing fronts (Hay, 2008) that facilitated better ventilation of the deep ocean (Gale, 2011).

Interestingly, the primary cause driving the Maastrichtian climate change and finally leading to the K-Pg extinction event may have come from space. Nimura *et al*. (2016) argue that our solar system encountered one of the dark clouds located within the Milky Way Galaxy disk during the last 8 Myr of the Cretaceous. This resulted in a sunshield effect, hence, global cooling, sea-level fall and other large-scale phenomena. The idea is based on the observation of an increasing extraterrestrial index, reflected in the abundance of iridium in Maastrichtian pelagic sediments, and fits well with the dinosaur genus survival rate, proposed by Sloan *et al*. (1986) for the same time period.

Nevertheless, despite the initial causes, combined palaeontological and stable isotope evidence indicate cold to warm greenhouse and reverse changes in climate during the Maastrichtian (see also e.g., Barrera, 1994; Dubicka and Peryt, 2012; Dameron *et al*., 2017; Mateo *et al.,* 2017).

This paper focuses on calcareous nannoplankton assemblages and their changes through time that may have been driven by the assumed Maastrichtian climate changes (see also Linnert *et al*., 2016). Moreover, in the uppermost part of the section studied the K-Pg boundary interval already has been recognized and is only one of several identified in the Outer Carpathians (Gasiński and Uchman, 2011). Therefore, the stratigraphy of the Bąkowiec section also is challenged here.

GEOLOGICAL SETTING

The section studied is situated in the Skole Nappe, the most external nappe of Polish Outer Carpathians (Fig. 1). This nappe embraces a series of detachments and dislocations as a result of Miocene folding and northward thrusting (Wdowiarz, 1949). The section mostly consists of flysch deposits and represents the Ropianka Formation, formerly known as Inoceramian Beds, spanning the Turonian through the Paleocene (Kotlarczyk, 1978) and overlain by the Eocene Variegated Shale Formation (Rajchel, 1990). The deposits of the Ropianka Formation accumulated in the deep-sea part of the Skole Basin, i.e. the northern part of the Tethyan Ocean, bordering the East European Platform (e.g., Bromowicz, 1986; Łapcik *et al*., 2016; Łapcik, 2018).

The section is a composite section that encompasses a set of isolated outcrops of the Ropianka Formation, scattered between the villages of Husów and Handzlówka and located on the southern slope of Patria Hill (426 m a.s.l.), in the Bąkowiec Forest. The outcrops can be found in the left bank of the Handzlowski Potok Stream and along its unnamed right tributary (Fig. 1). All beds sampled are dipping uniformly in a SE direction, indicating a stratigraphically continuous, monoclinal structure for this part of the Husów Thrust Sheet. The main and stratigraphically uppermost part of the section studied (GPS coordinates: N49°58′41″; E22°14′51″; ±15m) reveals a 4-m-thick series of beds, thrust over red-coloured Eocene Variegated Shales of the lower thrust sheet (Wdowiarz, 1949).

In general, the section studied is composed of medium to thick turbiditic beds of calcareous sandstones, interbedded with grey to bluish grey marls, marly siltstones and mudstones in the lower part and calcareous shales in the upper part. The sandstones are fine-grained, mostly without depositional structures (singly Tb or Tc Bouma divisions) with numerous calcite veins. The mudstones predominate over sandstones in mostly a 2:1 ratio.

MATERIAL AND METHODS

The set of hemipelagic soft marls or calcareous shales sampled by authors during the fieldwork were used in the preparation of nineteen microscope slides by means of the simple smear slide technique (Bown and Young, 1998). The slides were used in the qualitative and semi-quantitative examination of calcareous nannofossils under a Nikon Eclipse E600 Pol cross-polarised light microscope at 1000x magnification. The semi-quantitative data used in this study concern the abundance of given nannofossil taxon in relation to the abundance of other taxa recognized in the assemblage, represented by 300 specimens counted (its percentage; see Bown and Young, 1998).

The calcareous nannofossil data then were used in the calculation of the Temperature Index (TI; see Watkins and Self-Trail, 2005), the Nannofossils Index of Productivity (NIP; see Eshet and Almogi-Labin, 1996) and the biodiversity Shannon Index (SI; see Shannon and Weaver, 1949). Owing to the non-continuous occurrence of a few taxa throughout the section, their absence with values of 0 are replaced with 0.001 in order to obtain the continuity in data necessary for similarity calculations.

Temperature Index (TI)

TI values were estimated on the basis of the mutual relationships of warm- *vs*. cool-/cold-water nannofossil taxa in every sample slide. For this estimation, *Watznaueria barnesiae* (Black), *Ceratolithoides* spp. and *Micula murus* (Martini) were considered to represent warm-water taxa, and *Ahmuellerella octoradiata* (Górka), *Arkhangelskiella cymbiformis* Vekshina, *Eiffellithus turriseiffelii* (Deflandre), *Micula staurophora* (Gardet) or *Prediscosphaera cretacea* (Arkhangelsky) cool-water taxa (see Bukry, 1973; Thierstein, 1976, 1981; Wise, 1983; Watkins, 1992; Watkins *et al*., 1996; Bergen and Sikora, 1999; Less, 2002). The TI calculation was carried out using the formula proposed by Watkins and Self-Trail (2005): TI = [(% warm taxa) /(% warm taxa + % cold taxa)] × 100.

Nannofossil Index of Productivity (NIP)

The NIP was calculated according to the formula used by Eshet and Almogi-Labin (1996 and references therein). The nannofossil observations allowed the authors to recognize two groups, characterizing productivity conditions: (I) a low-productivity group that consists of *Eiffellithus* spp. (*E. gorkae* Reinhardt, *E. turriseiffelii* or *E. parallelus* Perch-Nielsen), *Microrhabdulus decoratus* Deflandre and *Prediscosphaera* spp. (*P. cretacea* or *P. grandis* Perch-Nielsen) and (II) a high-productivity group, including *Biscutum* spp. [*B. melaniae* (Górka) or *B. dissimilis* Wind and Wise]. The NIP value was computed as follows: NIP = Group II / Group I (log).

Shannon Index (SI)

In addition to the NOS, the Shannon Index (SI):

$$SI = -\sum_{i=1}^{s} p_i \ln p_i$$

(see Shannon and Weaver, 1949) was calculated to determine biodiversity changes in the calcareous nannofossil assemblage along the section studied. Furthermore, the $CaCO_3$ content, in compliance with the Scheibler volumetric method, as well as the $\delta^{13}C$ and $\delta^{18}O$ stable isotope ratios were measured for each rock sample. For the latter results, powdered rock samples were reacted with oversaturated 100% orthophosphoric acid at 70 °C in a Kiel II automated reaction system and measured with a Delta Plus isotope-ratio mass spectrometer at the Institute of Earth Sciences, University of Graz, Austria. The reproducibility of replicate analyses for standards (in-house and NBS 19) and sediment samples was better than ±0.1‰ for $\delta^{13}C$ and ±0.12‰ for $\delta^{18}O$. All carbonate isotopic values are quoted relative to VPDB. The multivariate method of R-mode cluster analysis (Anderberg, 1973; Tan *et al*., 2006) using the Pearson Correlation Coefficient (PCC) was computed for all data collected. Cluster analysis using PCC was performed only for those variables that show continuous (or almost continuous) occurrence throughout the section studied. The statistical calculations were made using the PAST data analysis package (Hammer *et al*., 2001).

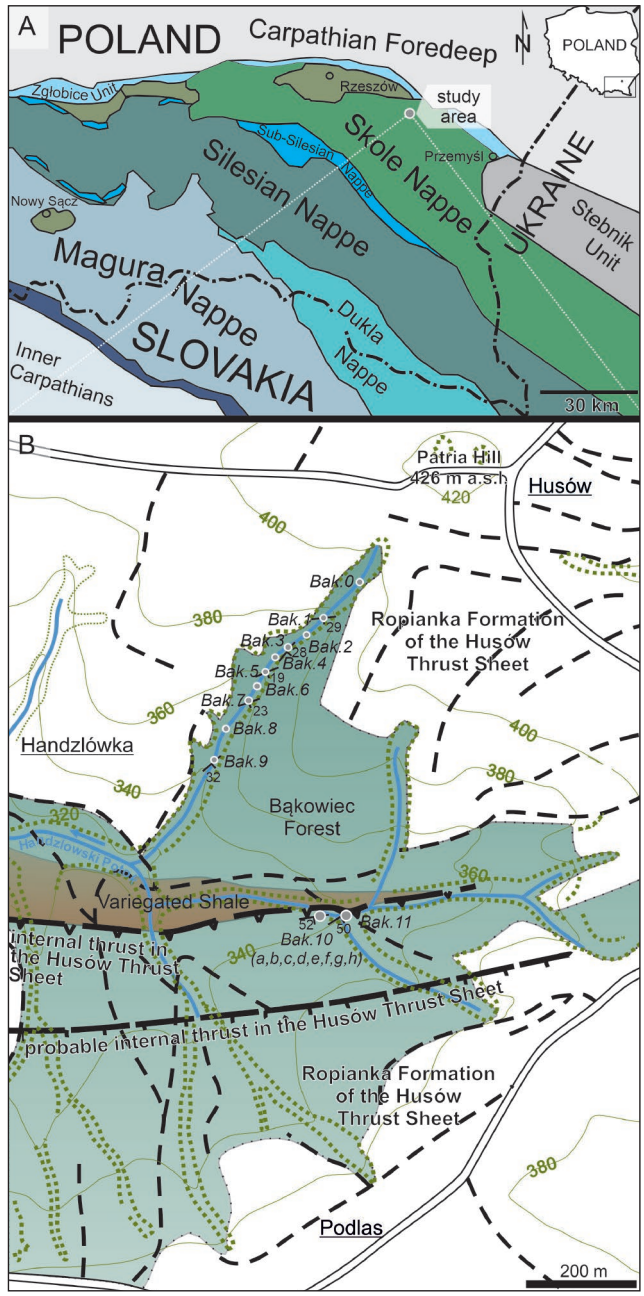

Fig. 1. Location map. **A.** Location of the study area in the Skole Nappe (modified after Książkiewicz, 1956). **B.** Map of the study area (modified after Gasiński and Uchman, 2011). Tectonic units and localization of Variegated Shale after Wdowiarz (1949). Place of sampling (Bak.0, etc.) with beds orientation.

RESULTS

Calcareous nannofossils

Forty-three species of twenty-seven genera of calcareous nannofossils were identified in the microscopic slides studied (Fig. 2; Tab. 1). This provides a fully statistically significant package of assemblages except for those from four slides, i.e. Bak.0, Bak.3, Bak.4, and Bak.10g, in which the nannofossil assemblage does not exceed 300 specimens. The number of species or taxa counted (NOS) varies from 10 in sample slide Bak.10g to 31 in Bak.0 (on average 22).

The state of preservation of the nannofossil assemblage was determined as the visual degree of recognizability of the specimen (see Kędzierski and Leszczyński, 2013). All assemblages studied (beside Bak.10g) represent a good-to-moderate or good state of preservation. Furthermore, no significant sign of dissolution or etching damage was noted as impacting on the taxonomic recognizability of specimens counted.

In general, sample slides contain moderately diverse nannofossil assemblages with the predominance of *W. barnesiae* and *M. staurophora*. Their combined contribution in assemblage total abundance varies from 34.7% in sample slide Bak.10g to 89.3% in Bak.11.

The less abundant taxa, such as *Arkhangelskiella* spp., *Broinsonia* spp., *Chiastozygus* spp., *Cribrosphaerella ehrenbergii* (Arkhangelsky), *Eiffellithus* spp., *Prediscosphaera* spp. and *Reinhardtites* spp., altogether constitute roughly 8.2% of the total assemblage (Bak.11) to 40.1% (Bak.2).

Accordingly, other taxa, such as *Arkhangelskiella* spp. (mostly *A. cymbiformis*), account for 10.6% of all taxa in sample Bak.2 to 0.3% in Bak.10h, *Broinsonia* spp. [*B. parca parca* (Stradner)*, B. enormis* (Shumenko)] 7.9% (Bak.4) to 1.0% (Bak.10b), *Chiastozygus* spp. (*Ch. synquadriperforatus* Bukry*, Ch. bifarius* Bukry) 0.3% (Bak.10e, Bak.10h) to3.5% (Bak.0), *C. ehrenbergii* 1.6% (Bak.11) to 11.8% (Bak.3), *Eiffellithus* spp. (*E. gorkae, E. parallelus, E. turriseiffelii*) 0.3% (Bak.11) to 7.6% (Bak.0), *Prediscosphaera* spp. (*P. cretacea, P. grandis*) from barren slides (Bak.10g, Bak.11) to 11.5% (Bak.2), *Reinhardtites levis* Prins and Sissingh from barren slides (Bak.2, Bak.3, Bak.6) to 6.7% (Bak.10g) (Fig. 4).

A rare occurrence of *A. octoradiata*, *Biscutum* spp. (*B. melaniae, B. dissimillis*), *M. decoratus*, *Ceratolithoides* spp. was noted as well.

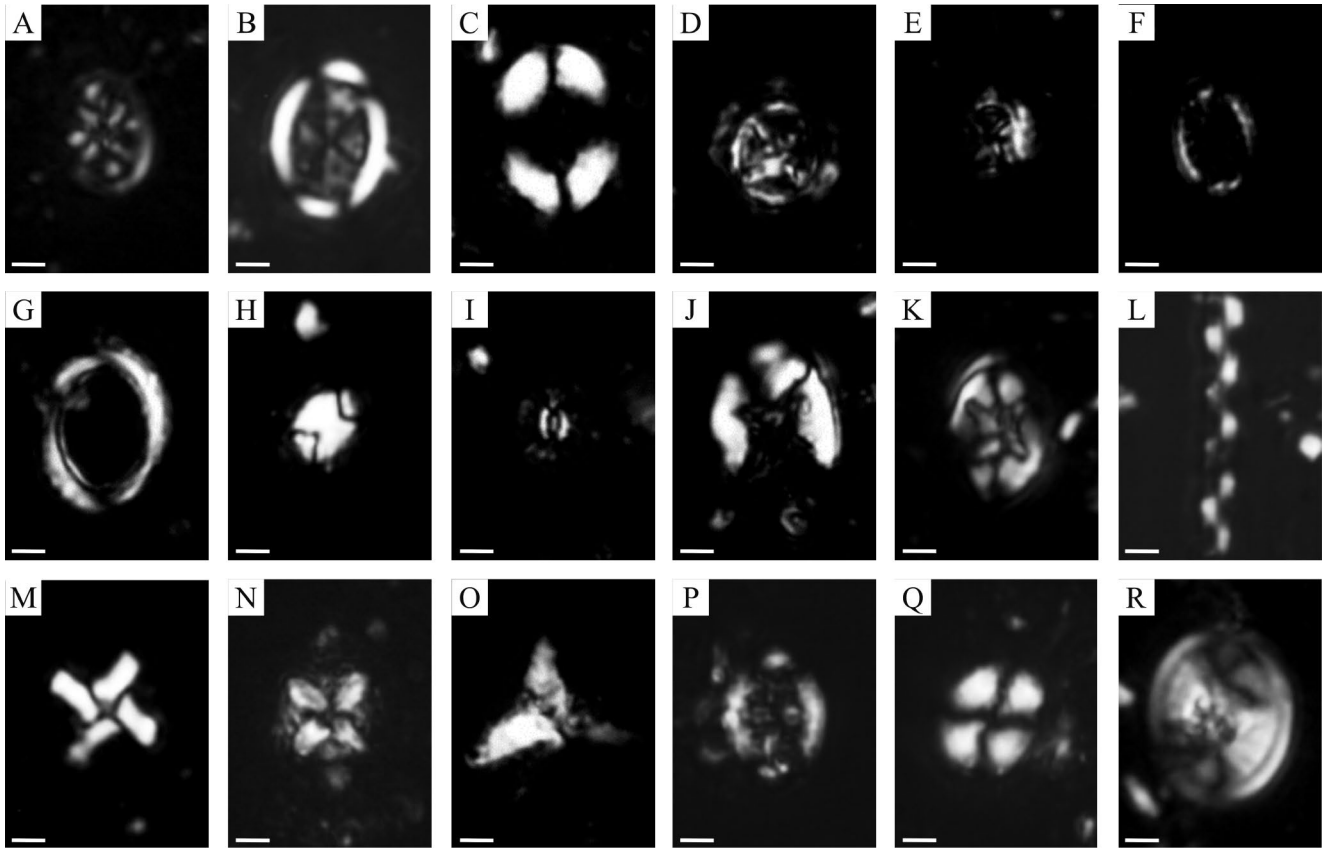

Fig. 2. Calcareous nannofossil in cross-polarized light. **A.** *Ahmuellerella octordiata*, sample Bak.0. **B.** *Arkhangelskiella cymbiformis*, sample Bak.10a. **C.** *Broinsonia parca parca*, sample Bak.1. **D.** *Prediscosphaera cretacea*, sample Bak.10b. **E.** *P. grandis*, sample Bak.9. **F.** *Cribrosphaerella ehrenbergii*, sample Bak.10c. **G.** *Loxolithus armilla*, sample Bak.10a. **H.** *Calculites obscurus*, sample Bak.10d. **I.** *Biscutum melaniae*, sample Bak.5. **J.** *Eiffellithus parallelus*, sample Bak.2 **K.** *E. turriseiffelii*, sample Bak.10c. **L.** *Microrhabdulus decoratus*, sample Bak.10a. **M.** *Micula prinsii*, sample Bak.10a. **N.** *M. staurophora*, sample Bak.11. **O.** *Uniplanarius trifidus*, sample Bak.10e. **P.** *Staurolihites* sp., sample Bak.10c. **Q.** *Watznaueria barnesiae*, sample Bak.10e. **R.** *Reinhardtites levis*, sample Bak.10d. The scale bar equals 2 μm.

TI, NIP and SI indexes

The TI value varies from 20.4 in sample Bak.2 to 62 in samples Bak.10e and Bak.10h. The highest values of TI are indicative of the upper part of section, where they reach about 50 or above, i.e. samples Bak.10a through Bak.10h. In contrast, in the lower part of the section that is characterized by the predominance of cold-/cool-water taxa, the TI values remain about 30, on average.

NIP values vary from –0.4 for the nannofossil assemblage in slide Bak.10h to –4.8 in Bak.2. The highest negative values (i.e. in Bak.2, Bak.10f, Bak.10g, and Bak.11) indicate assemblages with an absence of any high-productivity taxon (0 was replaced by 0.001 in these cases).

SI values oscillate between 1.165 in slide Bak.11 and 2.545 in Bak.0. The highest SI values of about 2 characterize the assemblages in the lower part of section for the most part. In contrast, a decreasing trend in values is observed in the upper part, starting from sample Bak.8 and upwards.

Stable isotopes

The bulk rock $\delta^{13}C$ stable isotope ratio values vary from 0.7 in samples Bak.1 to 2.3 in sample Bak.6 and for $\delta^{18}O$ from –4.0 (Bak.3) to –1.6 (Bak.6). The highest fluctuations in ratio of both carbon and oxygen isotopes values occur in the bottom part of the section. The $\delta^{18}O$ isotope ratio values log shows two positive excursions at the base of the section studied, as follows: –3.8 value (Bak.0) shifts to –1.7 (Bak.2) and –4.0 (Bak.3) to –1.6 (Bak.6). The above part of the section is characterized by a continuous slight decrease in the stable oxygen isotope ratio values. Likewise, the carbon stable isotope ratio values log also shows two positive excursions in the lower part of the section: 0.8 (Bak.4) to 2.3 (Bak.6) and 1.0 (Bak.9) to 2.0 (Bak.10a), and then they gradually increase upwards. The latter excursion in oxygen isotope ratio values follows the positive shift in the value of the $\delta^{13}C$ isotopes ratio.

Statistical analysis

The statistical analysis relies on the multivariate method of R-cluster analysis (Anderberg, 1973; Davis, 1986), of the variables representing data continuity, or almost continuity, along the section studied. The sixteen variables correlated in this study are: NIP, SI, NOS, $CaCO_3$, TI, $\delta^{13}C$, $\delta^{18}O$ as well as the abundance of the nannofossil genera (*Cribrosphaerella, Eiffellithus, Arkhangelskiella, Broinsonia, Chiastozygus, Micula, Watznaueria, Prediscosphaera, Reinhardtites,*). The variables similarity, using the Pearson correlation coefficient and the pair-group (UPGMA) algorithm were calculated for their clustering (Anderberg, 1973; Tan *et al*., 2006). Cluster analysis is a nonparametric method and does not need to make any assumptions on population distribution. Additionally, the grouping of variabilities was imposed on 0.3 level of similarity coefficient, splitting variabilities into three separate groups: the first cluster (I) containing *Cribrosphaerella* spp., SI, *Eiffellithus* spp., NOS, the second cluster (II) including *Arkhangelskiella* spp., *Prediscosphaera* spp., *Broinsonia* spp., $CaCO_3$, *Chiastozygus* spp. and the third (III), which consists of *Reinhardtites* spp., *Watznaueria* spp., TI, $\delta^{13}C$, $\delta^{18}O$ (Fig. 3). The other two variabilities accordingly indicate for NIP r = 0.13 and *Micula* spp. r = –0.07 value variance, banning these from clusters by assumed a 0.3 grouping level. The cophenetic correlation value reaches CPCC = 0.7616, hence the clustering can be considered as a good/reliable (Farris, 1969).

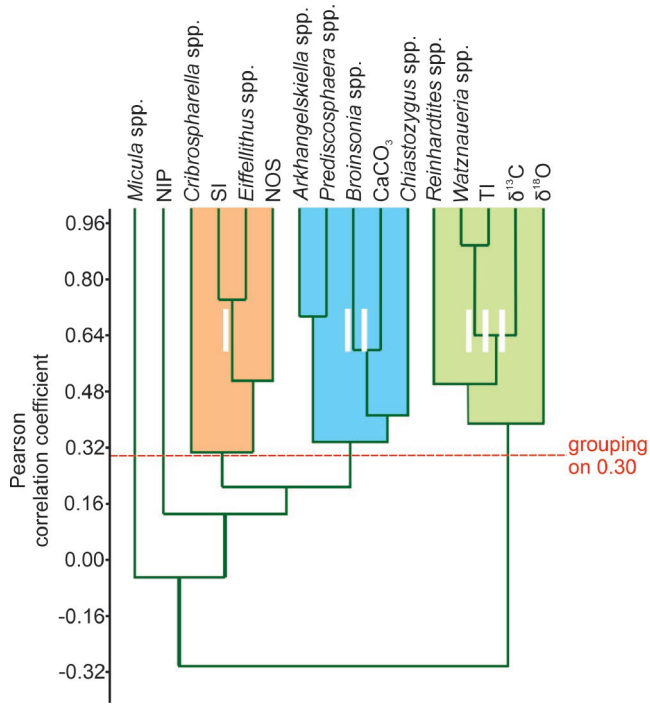

Fig. 3. Dendrogram showing the results of R-mode cluster analysis from the Bąkowiec section; NIP – Nannofossils Index of Productivity, SI – Shannon Index, NOS – Number of Species, TI – Temperature Index.

DISCUSSION

Taphonomy

Owing to its tiny dimension and fragile structure, calcareous nannoplankton are commonly considered to be microfossils particularly susceptible to dissolution and/or overgrowth during their pre- and post-burial history. The latter property especially affects nannofossil damage/dissolution resistance (see Steinmetz, 1994; Bown and Young, 1998). Experimentally obtained, the nannofossil dissolution index displayed a taxa dissolution resistance continuum, starting from solid, cubic forms, such as *Micula* spp., through coccoliths with an unperforated central area (*W. barnesiae*) and ending with fragile muroliths, such as *Zeugrhabdotus* spp. (Thierstein, 1980). Therefore, the dominance of dissolution resistance taxa in a nannofossil assemblage can evidences a taphonomic filtering. For instance, Roth and Bowdler (1981) ascertained that nannofossil assemblages containing 40% or more *Watznaueria* spp. are influenced by the dissolution effect. However, this taxon has been recognized as *r*-selected strategy life one, therefore, its dominance can be

Table 1

The distribution of nannofossils in the Bąkowiec section.

Sample	Specimens counted	Number of sepciesa	*Ahmuellerella octoradiata*	*Ahmuellerella* sp.	*Arkhangelskiella confusa*	*Arkhangelskiella cymbiformis*	*Arkhangelskiella* sp.	*Biscutum dissimilis*	*Biscutum melaniae*	*Biscutum* sp.	*Broinsonia parca parca*	*Broinsona enormis*	*Broinsonia* sp.	*Calculites obscurus*	*Ceratolithoides* sp.	*Chiastozygus synquadriperforatus*	*Chiastozygus bifarius*	*Chiastozygus* sp.	*Cribrosphaerella ehenbergii*	*Eiffellithus gorkae*	*Eiffellithus parallelus*	*Eiffellithus turriseiffelii*	*Gartnerago segmentatum*	*Gorkaea obliqueclausus*	*Loxolithus armilla*	*Microrhabdulus decoratus*	*Micula murus*	*Micula preamurus*
Bak.0	198	32	3.5			2.0	1.0	1.0		1.5	5.6			2.0	0.5	1.5	0.5	1.5	6.1			7.6						0.5
Bak.1	330	28	0.6	0.6		4.5	2.7	0.6		0.6	4.2			1.2	0.3	0.6		0.6	2.4	0.3		0.9	0.3			1.5		0.3
Bak.2	339	23	0.9		0.6	7.1	3.0				2.7	0.3				0.3		0.3	7.7		1.8	5.3				1.2		0.3
Bak.3	93	15		1.1		2.2	1.1			2.2	3.2		1.1					1.1	11.8			4.3						
Bak.4	178	16				6.7	3.4			0.6	5.1		2.8			1.7		0.6	8.4		1.1							
Bak.5	338	25	0.9			4.4		1.5	1.2	0.9	1.5		0.3	1.5		1.5		1.2	6.2	0.9		5.3				0.9		
Bak.6	317	18				6.0	1.3		0.3		2.5		0.6	0.3		0.6		0.6	5.0			0.9				0.6		
Bak.7	324	20				5.6	0.3		0.3		3.7		0.6	0.9		1.9		0.3	4.6			1.9				0.3		
Bak.8	326	29	0.6	0.3	0.3	5.5	2.4		0.3	0.3	3.4		1.5	1.2		0.3		0.9	5.5			1.8				0.3		
Bak.9	328	23	1.5		0.6	5.2	2.4		0.3		1.2		1.8			0.6		0.3	6.1	0.3		2.7				0.9		
Bak.10a	315	30	0.6			0.6				0.3	1.9			0.6		0.3		0.6	6.7	0.3		4.1			0.3	1.0		
Bak.10b	310	22				0.3	0.3	0.6			1.0			0.3				1.3	6.1	0.3		2.6						
Bak.10c	321	27	0.3	0.6		1.6	1.2			0.3	2.2		1.6	0.9				0.9	9.7	0.3		5.0		0.3				
Bak.10d	331	23	0.6				0.6			0.3	3.6		0.3	1.8				0.6	7.9			6.0	0.3				0.3	
Bak.10e	339	23		0.3		0.3	0.3		0.3	0.3	3.2		0.3			0.3			6.5			2.1						0.3
Bak.10f	313	22	0.6	0.6		1.0	0.3				1.9		1.3	1.0				1.0	6.1			2.6				0.3		
Bak.10g	43	10					2.3						7.0					2.3	7.0			7.0						
Bak.10h	320	20	0.3			0.3				1.3	3.4		0.3	0.6				0.3	6.3	0.3		1.6				0.3		
Bak.11	317	15		0.3		0.6					0.9		0.6	0.6				0.6	1.6	0.3						0.3		

Sample	*Micula prinsii*	*Micula staurophora*	*Misceomarginatus pleniporus*	*Markalius inversus*	*Placozygus fibuliformis*	*Prediscosphaera cretacea*	*Prediscosphaera grandis*	*Prediscosphaera* sp.	*Psykhosphaera firthii*	*Quadrum* sp.	*Reinhardtites levis*	*Reticapsa angustiforata*	*Reticapsa crenulata*	*Reticapsa surirella*	*Saurolithites mielnicensis*	*Saurolithites imbricatus*	*Saurolithites zoensis*	*Staurolithites* sp.	*Tranolithus minimus*	*Uniplanarius trifidus*	*Uniplanarius gothicus*	*Uniplanaris* sp.	*Watznaueria bernesae*	*Watznaueria quadrirradiata*	*Zegrhabdotus embergerii*	*Zeugrhabdotus praesigmoides*	*Zeugrhabdotus sigmoides*	*Zeugrhabdotus* sp.
Bak.0		29.8	0.5		0.5	1.0	2.0	2.5	0.5		2.0	1.0				0.5		0.5		0.5	0.5		19.2	2.0	1.0			1.0
Bak.1		54.2		0.6	0.6	0.3	3.0	2.1			0.3							0.3			0.6		15.5					
Bak.2		40.7			0.3		9.4	1.8	1.2				0.3				0.9	0.3					13.9					
Bak.3		46.2					3.2		4.3	1.1												1.1	16.1					
Bak.4		34.3					5.1	1.7			1.1									0.6			27.0					
Bak.5		30.2			1.2	0.3	8.9	2.4	0.9		0.3		0.3										26.6			0.6		0.3
Bak.6		51.1			0.3	0.3	3.5	0.3					0.3										25.2					
Bak.7		48.8			0.3	0.3	5.6	1.5			0.6										0.3		21.9					0.3
Bak.8		28.8			1.5	0.3	4.6	1.5	0.3		0.9		0.3				0.3	0.3					35.3	0.3				0.6
Bak.9		43.0			0.9	0.3	6.7	2.7			0.6							0.3					20.4				0.3	0.6
Bak.10a	0.3	23.2		0.3	0.6	0.3	4.4	1.3	1.3		2.2	1.3	0.6		0.3			0.6		0.3	0.6		43.5	1.0				0.3
Bak.10b		34.5			0.3	0.3	2.9	1.3		0.3	2.9	0.3								0.3	0.3	0.6	42.6					0.3
Bak.10c		29.0		0.3			0.9	0.9	0.3		4.4	0.3	0.6					0.6		2.5	0.3		34.3	0.3				0.3
Bak.10d		28.1			0.6		2.4	0.9			6.3		0.3							0.9	0.6	0.3	36.3	0.3				0.6
Bak.10e		28.6		0.3			0.6	0.6	0.3		1.8	0.6	0.3					0.3		1.2			51.0					0.3
Bak.10f		28.4			1.3	0.3	1.9	1.6			3.5									0.3	0.6	0.3	44.7					0.3
Bak.10g		20.9									11.6												37.2	2.3			2.3	
Bak.10h		28.8			0.3		0.3	0.3			2.8			0.3						1.6			50.3					0.3
Bak.11		56.5									3.5								0.3				32.8				0.6	0.3

also an effect of environmental conditions that are hostile for other taxa (Less *et al*., 2004). Moreover, more recent studies provide evidence that nannofossil assemblages can preserve the primary biocenosis composition well because they are more resistant to dissolution than other microfossils, for instance, foraminifera (Chiu and Broecker, 2008; Hassenkam *et al*., 2011). The most solution-prone taxa, such as *Zeugrhabdotus* spp. and *Staurolithites* spp. (Thierstein, 1980; Roth and Bowdler, 1981; Bown and Young, 1998), have been found along dissolution-resistant taxa, i.e. *Micula* spp. in the nannofossil assemblages studied. This indicates little or no taphonomic filtering of the calcareous nannoplankton assemblages considered in this study. However, the ratio of *M. staurophora* and *W. barnesiae* abundance changes upward, in favour of the latter species. A similar trend, interpreted as an environmental signal, was described in the Eastern Carpathians of Romania (Bojar and Bojar, 2013).

Biostratigraphy

The significance of the Bąkowiec section relies on the claim that this is one of a few flysch localities in the Outer Carpathians, where the K-Pg boundary interval so far was identified (Gasiński and Uchman, 2011). The foraminifera-based biostratigraphy of the Bąkowiec section consists of the Maastrichtian *Gansserina gansseri* (Boli) and *Abathomphalus mayaroensis* (Boli) as well as early Paleocene P1 biozones. Additionally, the *Racemiguembelina fructicosa* Zone, as the Partial Range Zone within the lower part of *A. mayaroensis* Zone, was recognized. Furthermore, the K-Pg boundary interval was determined in the two turbidite beds that are a forty-cm-thick part of the fifteen-metres-thick section (Gasiński and Uchman, 2011). The interval is marked there as an upper part of the section and placed in between interturbidites, yielding the last appearance of *A. mayaroensis* and the first appearance of *Subbotina cancellata* (Blow), *S. triangularis* (White) and *Eoglobigerina* cf. *edita* (Subbotina) planktic foraminifers, respectively (Gasiński and Uchman, 2011). In this chapter, the calcareous nannofossil stratigraphy of the Bąkowiec section is discussed with special emphasis on the uppermost Maastrichtian and alleged transition to the K-Pg boundary interval.

The most useful calcareous nannofossil stratigraphic marker species recorded in the section studied is *Micula prinsii* Perch-Nielsen. This species is considered to be an indicator of very uppermost Maastrichtian (e.g., Perch-Nielsen, 1981; Henriksson, 1993; Burnett, 1998), being the index species of the latest Maastrichtian calcareous nannoplankton zone in the many zonation proposed so far, e.g. CC26b by Sissingh (1977), *Micula prinsii* Zone by Perch-Nielsen (1981) or UC20d^{TP}, recently in the most widely used Burnett's zonation (1998). Owing to the lower and upper boundaries, all these zones are defined by the first occurrence (FO) of *M. prinsii* and the K-Pg boundary, respectively; they can be regarded as chronostratigraphic equivalents. The FO *M. prinsii* is usually recorded close to the base of Chron C29r and the last Cretaceous *Discoscaphites iris* ammonite Zone (Larina *et al*., 2016). However, the stratigraphic position of FO *M. prinsii* in sections representing different palaeobioprovinces is diachronous and relies on palaeoclimate fluctuations (Gardin, 2002; Thibault and Husson, 2016). It seems that *M. prinsii* first occurred in lower palaeolatitudes and then migrated poleward and back, depending on climate shifts. Therefore, the timespan of the latest Maastrichtian calcareous nannoplankton zone differs between palaeolatitudes, ranging from 220 Kyr to 1.2 Myr (see Hennebert, 2012, 2014; Thibault and Husson, 2016). Remarkably, Burnett (1998) used this species as an index nannofossil for the Tethys, hence, its occurrence out of that province or at its marginal part can be ephemeral, depending on climate warming and/or the inflow of warm, tropical water masses. Nevertheless, the presence of *M. prinsii* in the Bąkowiec section indicated the base of at the most a 1-Myr interval of the topmost Cretaceous above its FO, i.e. sample Bak.10a (equivalent of sample Bak.12 in Gasiński and Uchman, 2011).

The rock samples taken from below FO *M. prinsii* do not provide any index nannofossil species used in Burnett's (1998) UC^{TP} zones, i.e. *Lithraphidites quadratus* (UC20a^{TP} Zone) or *Ceratolithoides kamptneri* (UC20c^{TP}). Moreover, *Micula murus*, the index species for the UC20b^{TP} Zone first occurs above FO *M. prinsii,* i.e. in rock sample Bak.10d. The occurrence of both species in the upper part of the section studied and the contemporaneous absence of other Tethyan index species in the section below, i.e. *C. kamptneri* Bramlette and Martini and *L. quadratus* Bramlette and Martini, may be interpreted as a record of the environmental changes that occurred during the latest Maastrichtian (e.g., Thibault and Husson, 2016). This means that samples Bak.10a and Bak.10d may represent the global warming period of the late Maastrichtian, shortly before the K-Pg boundary, that is the last ~370 Kyr of that age (see Thibault and Husson, 2016). Consequently, the samples from below Bak.10a represent the cooler time of the Maastrichtian (lower/upper Maastrichtian) with the predominance of Boreal or temperate nannofossil assemblages (see the text below).

K-Pg boundary

The Outer Carpathians deep-sea flysch facies is characterized by an incomplete sedimentary record, affected by the erosional activity of turbidity currents. As a result, this sequence of flysch rocks records a relatively small portion of time and consists mostly of stratigraphic gaps, namely "more gap than record", as already noted by Barrell in 1917 (see also Miall, 2014). Therefore, the K-Pg boundary interval in the Bąkowiec section, as defined by Gasiński and Uchman (2011), indicates a record of the time that passed between the last and first occurrences of *A. mayaroensis* and *S. cancellata*, *S. triangularis*, *E.* cf. *edita*, and the beds yielding these taxa are a record of random events that happened between their appearances. This could have happened, but did not have to happen during the K-Pg boundary interval.

On the other hand, the chance of finding evidence of the K-Pg boundary, such as a rusty layer (see Molina *et al.,* 2006), is much smaller than, for instance, that of finding a record of Deccan volcanic activity, lasting for several hundred Kyr of the latest Maastrichtian. Also, recognition of the K-Pg boundary interval, defined as a part of stratigraphic

record between the last and first occurrences of given taxa (see Gasiński and Uchman, 2011), i.e. without pointing out any interval index fossil, is questionable, because such a definition of the K-Pg boundary interval can be applied to any potential section or rock sample barren of fossils.

Furthermore, the reliability of the chronostratigraphic position of the K-Pg boundary that was determined on the basis of taxa vulnerable to environmental changes is doubtful. This especially concerns *A. mayaroensis*, which is considered a stenothermic, K-strategy species, susceptible to climate change. Its occurrence depends locally on environmental stress that can exclude this fragile species from the foraminifera assemblage (see Keller and Abramovich, 2009). Therefore, the disappearance of *A. mayaroensis* cannot be a reliable indicator of age, but rather evidence of environmental change (see also Kędzierski *et al*., 2015). Similarly, for instance, the nannoplankton species *M. murus*, index fossil of UC20b^{TP} Zone, also is known as a low-latitude, warm surface taxon, migrating from low-to-high latitudes in accordance with Maastrichtian climate changes (Thibault *et al*., 2010).

In summary, considering calcareous nannofossils, the only reliable indicators of the early Palaeogene are the appearance of newcomer species or the abundance of *Thoracosphaera* spp. or *Braarudosphaera* spp. (see Burnett, 1998; Kędzierski *et al*., 2011). None of these features are observed in the nannofossil assemblages studied. Therefore, the presence of the last Maastrichtian nannofossil UC20d^{TP} Zone remains the only stratigraphic indicator identified and the presence of the K-Pg boundary interval cannot be confirmed.

Maastrichtian climate changes recorded in nannofossil assemblages

The analysis of calcareous nannoplankton has been used many times as a tool in environmental studies, especially for contemporaneous or Quaternary assemblages (e.g., Winter *et al*., 1979; Giraudeau, 1992; Ziveri *et al*., 1995; Kinkel *et al*., 2000). Applying nannofossils older than Quaternary as a plausible palaeoevironmental indicator is a kind of problematic due to estimation of their palaeoecological preferences (Young, 1994). Nevertheless, the ecological preferences of some calcareous nannofossil taxa are well recognized and they can be used as a helpful tool in environmental reconstructions (e.g., Eshet and Almogi-Labin, 1996; Lees *et al*., 2005; Watkins and Self-Trail, 2005; Sheldon *et al*., 2010; Pavlishina and Wagreich, 2012).

Before any considerations of the calcareous nannofossils as a tool for deciphering the Maastrichtian environment, a general view of that time should be mentioned. The environmental perturbations affecting Maastrichtian biodiversity have been the subject of many studies regarding their contribution to the end-Cretaceous mass extinction, which was presumably triggered by an extraterrestrial bolide impact (e.g., Li and Keller, 1998, 1999; Olsson *et al*., 2001; Thibault and Gardin, 2010). The record of the $\delta^{18}O$ stable isotopes ratio, measured in both planktic and benthic foraminifera (e.g., Barrera and Savin, 1999) or bulk rocks (e.g., Thibault *et al*., 2016), shows the course of temperature changes in the oceanic water-column throughout the Maastrichtian. In general, therefore, it may be assumed that the Maastrichtian was characterized by a gradually cooling climate, interrupted by two episodes of global warming prior to the K-Pg boundary. The first warming encompasses the upper part of UC18 throughout the lower part of the UC20 nannofossil zones and is called the early or mid-Maastrichtian Event (EME or MME). The second one, called the late Maastrichtian event (LME) is noted within UC20d Zone (Li and Keller, 1998, 1999; Nordt *et al*., 2003; Abramovich *et al.,* 2010; Sheldon *et al*., 2010; Thibault and Gardin, 2010). There are lines of evidence that the LME warming passed into a cooler time, with a ~2 °C drop in temperature, about 100 kyr before the K-Pg boundary (e.g., Barrera and Savin, 1999; Li and Keller, 1998; Hart *et al*., 2005). The cause of the LME is often linked to Deccan volcanic activity (e.g., Pardo and Keller, 2007, 2008; Keller, 2008; Tantawy *et al*., 2009). However, other factors also can be considered (Frank and Arthur, 1999; Keller, 2005; Thibault and Gardin, 2010).

Furthermore, regarding calcareous nannoplankton, the Maastrichtian was the only time in the Mesozoic life-history of this group, when its species richness distinctively declined. That is, the preceding Campanian time evidenced its highest number of 149 species, followed by a slight decrease to 131 in the early Maastrichtian and an eventual drop to merely 9 species that survived the end-Cretaceous extinction event (see Bown *et al*., 2004). However, this roughly exponential trend can be challenged when examined in greater detail. For instance, Thibault and Husson (2016) showed periodic variation in the diversity of nannofossil assemblages during the late Maastrichtian. The high-diversity assemblages were replaced by low-diversity ones and the reverse, in relation to supposed climatic changes occurring during the latest Maastrichtian (UC20 Zone). Moreover, a comparison of data from different palaeolatitudes shows that the low-latitude sites (i.e. Tethys) recorded an additional warm period about 30–40 kyr before the K-Pg boundary, not detected at Boreal or Indian Ocean (high-latitude) sites. The last Maastrichtian climatic changes visible in nannofossil assemblage diversity variations are assigned solely to the UC20d^{TP} Zone, i.e. above the FO *M. prinsii* (Thibault and Husson, 2016).

In this study, the semi-quantitative calcareous nannofossil data allowed calculation of environmental indicators as follows: Temperature Index (TI), Nannofossil Index of Productivity (NIP) and Shannon Index (SI, see chapter above) (Figs 4, 5).

The first indicator (TI), showing the ratio of percentages of warm/cold (cool-)-water taxa, splits the section studied into two parts. The lower part, embracing samples Bak.0–Bak.9, is characterized by the dominance of cold-/cool-water taxa in nannofossil assemblages (>50%), whereas assemblages from the upper part (Bak.10a–h) are dominated by warm-water taxa. In the lower part of the section, one exception is made for sample Bak.8 showing 48.7% TI value, which seems to be a result of the increasing abundance of *W. barnesiae,* a warm-water taxon, sensitive to temperature fluctuations. In contrast, the upper part of the section (Bak.10a–h) reveals twofold higher TI values than the lower one. The increase of TI values upward section,

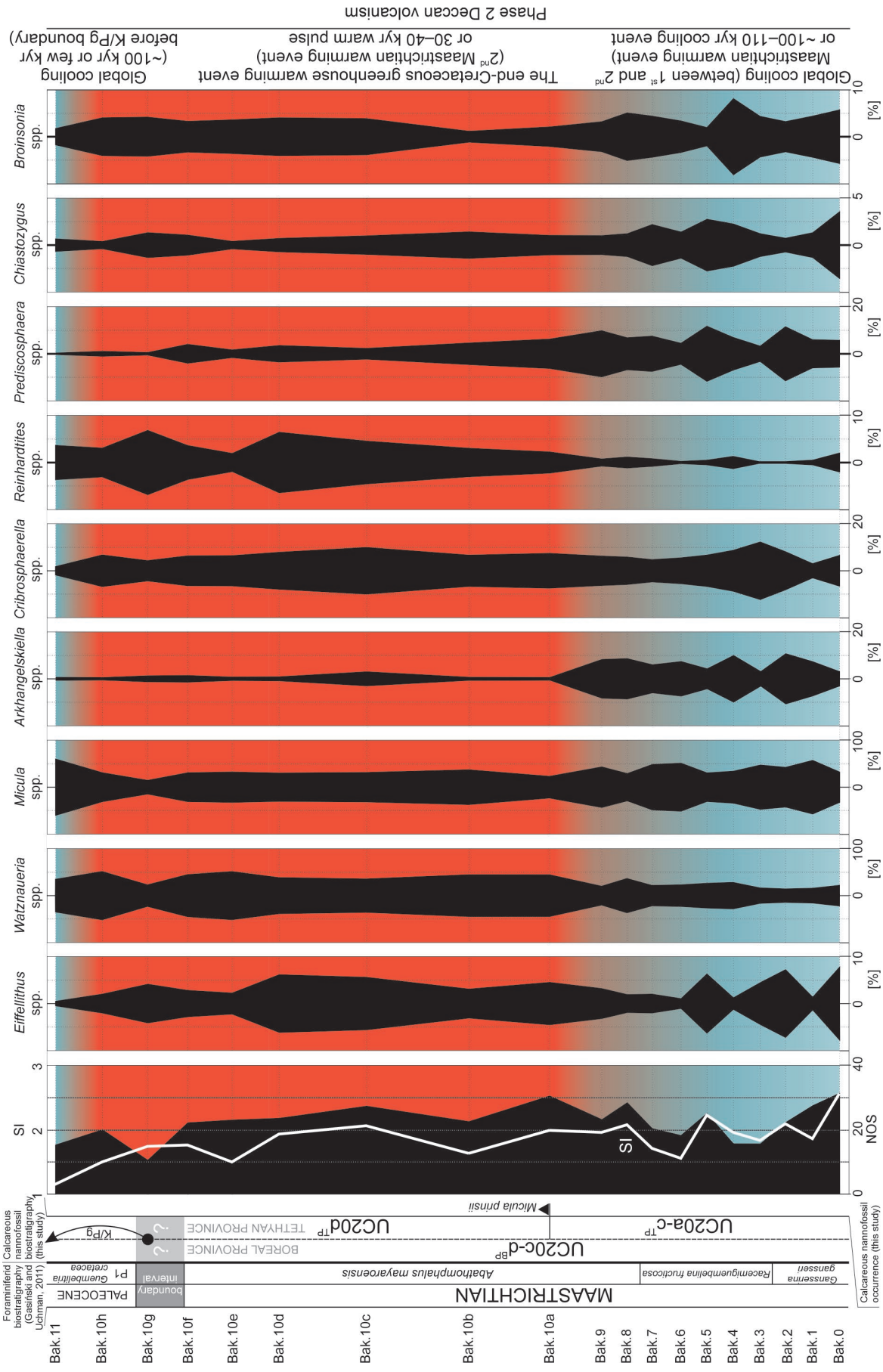

Fig. 4. The percentage of the main calcareous nannofossil groups with SI and NOS changes in the Bąkowiec section. Temperature conditions estimated by TI (blue highlight – predominance of cool-water assemblages, red highlight – predominance of warm-water assemblages).

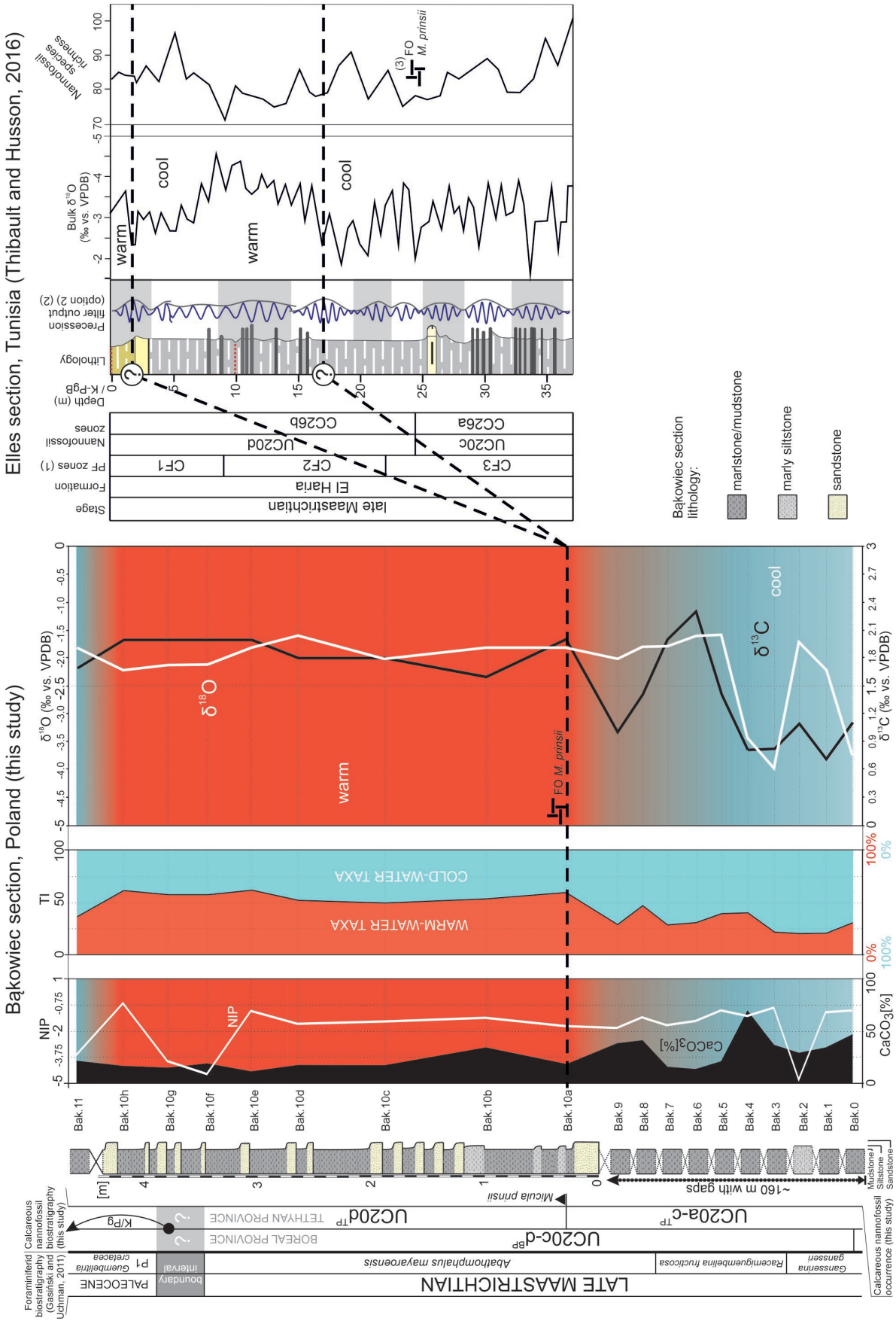

Fig. 5. Late Maastrichtian changes in bulk $\delta^{13}C$ and $\delta^{18}O$, in the $CaCO_3$ content, and in NIP and TI in the Bąkowiec section (Poland) with foraminiferid biostratigraphy (Gasiński and Uchman, 2011). Comparison to Elle section in Tunisia (Thibault and Husson, 2016 – (1), (2), (3) references and explanations therein). Black dashed line – correlation to base of warm period about 30–40 kyr or ~250 kyr (Sprain *et al*., 2019) before K-Pg boundary.

accompanied by the increasing abundance of *W. barnesiae,* and appearance of low-latitude *M. prinsii* may be interpreted as a record of end-Cretaceous warming preceding the K-Pg boundary event, linked to expansion of warm Tethyan water into northern basins (e.g., Sheldon *et al*., 2010; Thibault and Gardin, 2010). The species *M. prinsii* is considered a low-latitude taxon, never recorded in the Boreal province. It rarely was found in the Outer Carpathians (Jugowiec-Nazarkiewicz, 2007; Bojar and Bojar, 2013) and its sole appearance in the northern Carpathians basins seems to be related to the most eruptive phase of Deccan volcanism, which coincides with the range of the UC20d^{TP} Zone (Sprain *et al.,* 2019) or to the additional warming period 30–40 kyr before the K-Pg boundary, postulated by Thibault and Husson (2016; Fig. 5).

The NIP indicator describes the level of primary production of the upper part of water column. The positive or slightly negative NIP values mean an enhanced level of productivity, while values below –2 indicate low primary production (see Eshet and Almogi-Labin, 1996). In the section studied, NIP values lower than –2 are seen in samples Bak.2, Bak.10f, Bak.10g and Bak.11, indicating low-production assemblages, whereas the rest of the values can be interpreted as the record of a moderate level of primary production, slightly decreasing through time, i.e. between samples Bak.3 and Bak.10d, where the NIP values become progressively smaller. This decreasing trend of NIP is accompanied by increasing trend in TI that may evidence of weakening influence of fertile, cold Boreal waters in favour of the Tethyan ones during the UC20d^{TP} Zone warming. The decrease in $CaCO_3$ content upward in the section and likewise NIP may indicate a direct linkage between these two parameters (Fig. 5).

The Shannon Index (SI) is a diversity measure, i.e. assemblages dominated by one or a few taxa are characterized by low SI values, in contrast to highly diversified ones. The low SI values revealed in the Bąkowiec section correlate with the NIP, indicating advancing eutrophication linked to enhanced Tethyan warm-water influence during the latest Maastrichtian. On the other hand, low SI values noted across the UC20d^{TP} Zone may be partly a result of acidification of surface water during the late Maastrichtian warming (the so-called dissolution interval; see Dameron *et al.,* 2017; Fig. 4).

The lowest $\delta^{13}C$ stable isotopes ratio values have been measured in the lower part of the section studied (Bak.0 through Bak.4 and then Bak.9). There are two positive shifts of $\delta^{13}C$ ratio noted below sample Bak.10b: the first occurs in the lower part of the *R. fructicosa* Zone (Bak.4 to Bak.6) and the second one falls into lower part of the *A. mayaroensis* Zone. These shifts may reflect two episodes of increasing primary production recognized in the Maastrichtian, i.e. MME and LME, respectively. The latter is more completely recorded in the section studied, owing to a continuous series of samples starting from Bak.10a through Bak.10h. The higher $\delta^{13}C$ values in this part, accompanied by low NIP and SI values and the dominance of *r*-selected *W. barnesiae* species also seem to be linked to a warming event, triggering a eutrophication and biocalcification crisis (e.g., Erba, 2004).

The $\delta^{18}O$ stable isotopes ratio value can be significantly altered, owing to carbonate dissolution and/or reprecipitation implying a diagenetic overprint, whereas the $\delta^{13}C$ ratio may reveal a pristine signal (e.g., Barrera and Keller, 1990). The low values of both $\delta^{18}O$ ratio and $CaCO_3$ [%] content may indicate a higher concentration of clay minerals that causes a sample to become more resistant (less permeable) to water-rock interaction causing eventual secondary migrations of oxygen stable isotopes. Therefore, samples from the bottom part of the section (e.g., Bak.0 or Bak.4) are more likely to be diagenetically altered than samples taken from higher levels. However, a decreasing number of *A. cymbiformis,* considered a cold-water species, in samples Bak.0, Bak.3 and Bak.4 also could be the result of water temperature rising that is recorded by the negative shift of the $\delta^{18}O$ ratio log (though, in contrast, TI values remain low in samples Bak.2 and Bak.3; Fig. 5).

Cluster analysis

The multivariate R-mode clustering combines several variables, such as: abundances of nannofossil genera with a continuous record, geochemical data ($\delta^{13}C$, $\delta^{18}O$, $CaCO_3$) and environmental indicators, i.e. TI, NIP, NOS and SI. As a result, three clusters have been recognized (Fig. 3).

Cluster I is described by a strong positive variance between SI and abundance of *Eiffellithus* spp. and lower similarity of this pair with NOS and the abundance of *Cribrosphaerella* spp. All these variables clustered here are related to meso-to-oligotrophic conditions.

Cluster II shows a strong correlation of *Arkhangelskiella* spp. (mostly *A. cymbiformis*) and *Prediscosphaera* spp., two taxa abundant in Boreal realm, as well as the next two *Broinsonia* spp. and *Chiastozygus* spp. The $CaCO_3$ content that has fallen into this cluster made a linkage between cold-water influences and carbonate production.

The strongest positive variance among the variables compared is shown in cluster III, i.e. between *Watznaueria* spp. abundance and TI. This cluster also embraces the stable isotopes ratio values and *Reinhardtites* spp. abundance variability. In contrast to cluster I, this one seems to group variables linked with meso-to-high productivity periods, related to changes in water column temperature (climate changes?) and/or taphonomic filtering.

In summary, the clusters revealed three groups of variables linked to different environmental settings, characterizing sedimentation in the Skole Basin during the Maastrichtian. These settings can be recognized as: (I) meso-to-oligotrophic, low-productivity waters dominated by K-selected species; (II) cold-water, Boreal influence waters related to lowstand and enhanced carbonate resedimentation; (III) warm-water, Tethyan influence, related to highstand and dissolution interval related to acidification (Fig. 6).

CONCLUSIONS

The flysch deposits of the Bąkowiec section yielded moderately to well-preserved calcareous nannofossil assemblages, comprising 43 species of 27 genera recognized here.

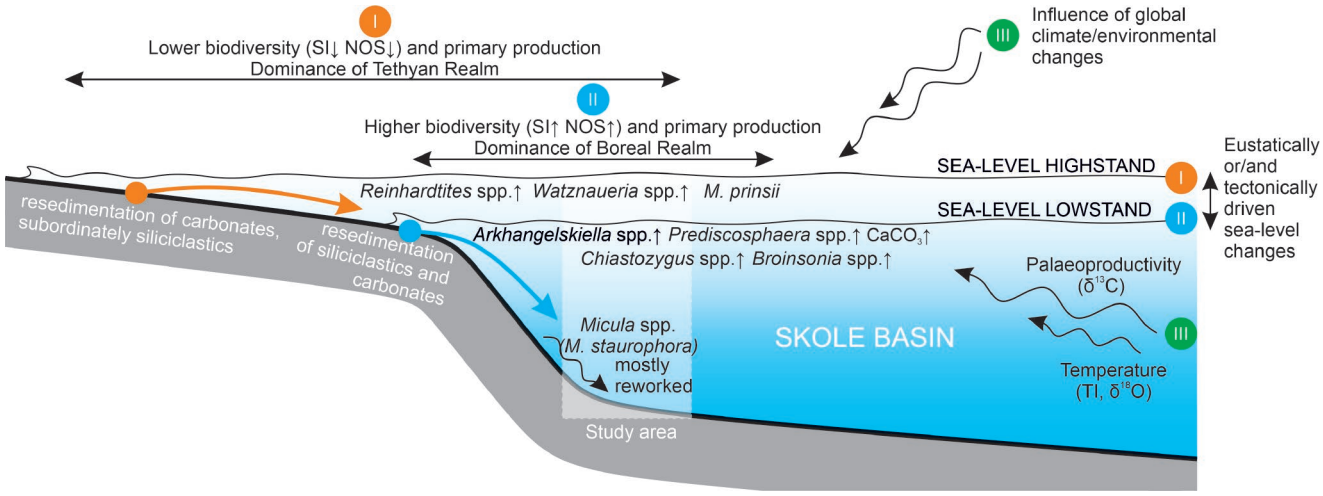

Fig. 6. The upper Maastrichtian depositional model for the Bąkowiec section containing three groups of different environmental settings affecting the Skole Basin.

The occurrence of the zonal marker species *Micula prinsii* defined the lower boundary of the UC20d^{TP} Zone, the last Maastrichtian nannofossil zone, which encompasses the last 4 metres of the section studied. The rest of the section is located below FO *M. prinsii* and falls into the lower-upper Maastrichtian UC20a-c^{TP} composite zone.

There is no evidence of the K-Pg boundary in the light of the investigation of calcareous nannofossils.

The calcareous nannofossil assemblage taxonomic composition analysis and stable isotope ratio changes revealed a climatic shift from cold to warm around the beginning of the UC20d^{TP}.

The UC20d^{TP} Zone recognized in the Bąkowiec section represents the last Maastrichtian warming event several, kyr before the K-Pg boundary, or the second warming pulse, about 250 kyr before the K-Pg boundary that may reflect the second phase of Deccan volcanism.

Cluster analysis of the combined nannofossil and isotope data show three clusters that are interpreted as groups of variables, characterizing three different environmental factors: trophic conditions and Boreal and Tethyan waters.

ACKNOWLEDGEMENTS

The authors are grateful to Roberto Silva Jr. (Rio de Janeiro, Brazil) and an anonymous reviewer for their critical reading of the manuscript and constructive comments. Michael Wagreich (University of Vienna, Austria) is acknowledged for help in obtaining isotopic data. The research was sponsored by funding from the Jagiellonian University and in part by the Polish National Science Centre (Grant No. UMO-2014/15/B/ST10/04229).

REFERENCES

Abrajevitch, A., Font, E., Florindo, F. & Roberts, A. P., 2015. Asteroid impact vs. Deccan eruptions: The origin of low magnetic susceptibility beds below the Cretaceous– Paleogene boundary revisited. *Earth and Planetary Science Letters,* 430: 209–223.

Abramovich, S., Yovel-Corem, S., Almogi-Labin, A. & Benjamini, C., 2010. Global climate change and planktic foraminiferal response in the Maastrichtian. *Paleoceanography,* 25: PA2201.

Alvarez, L. W., Alvarez, W., Asaro, F. & Michel, H. V., 1980. Extraterrestrial cause for the Cretaceous–Tertiary Extinction. *Science,* 208: 1095–1108.

Anderberg, M. R., 1973. *Cluster Analysis for Applications*. Academic Press, New York, 359 pp.

Barrell, J., 1917. Rhythms and the measurement of geologic time. *Geological Society of America Bulletin,* 28: 745–904.

Barrera, E., 1994. Global environmental changes preceding the Cretaceous–Tertiary boundary: Early–late Maastrichtian transition. *Geology,* 22: 877–880.

Barrera, E. & Keller, G., 1990. Stable isotope evidence for gradual environmental changes and species survivorship across the Cretaceous/Tertiary boundary. *Paleoceanography,* 5: 867–890.

Barrera, E. & Savin, S. M., 1999. Evolution of late Campanian-Maastrichtian marine climates and oceans. *Evolution of the Cretaceous Ocean-Climate System, GSA Special Paper*, 332: 245–282.

Belcher, C. M. & Hudspith, V. A., 2017. Changes to Cretaceous surface fire behaviour influenced the spread of the early angiosperms. *New Phytologist,* 213: 1521–1532.

Bergen, J. A. & Sikora, P. J., 1999. Microfossil diachronism in southern Norwegian North Sea chalks: Valhall and Hod fields. In: Jones, R. W. & Simmons, M. D. (eds), *Biostratigraphy in Production and Development Geology*. *Geological Society, London, Special Publications,* 152: 85–111.

Bojar, A.-V. & Bojar, H.-P., 2013. The Cretaceous-Paleogene boundary in the East Carpathians, Romania: Evidence from geochemistry, mineralogy and calcareous nannofossils. In: Bojar, A.-V, Melinte-Dobrinescu, M. C. & Smith, J. (eds), *Isotopic studies in Cretaceous Research*. *Geological Society, London, Special Publications,* 382: 105–122.

Bown, A. H. & Young, J. R., 1998. Techniques. In: Bown, P. R. (ed.), *Calcareous Nannofossils Biostratigraphy*. Kluwer Academic Publisher, Dordrecht, Boston, London, pp. 16–28.

Bown, P. R., Less, J. A. & Young, J. R., 2004. Calcareous nannoplankton evolution and diversity through time. In: Thierstein, H. R. & Bown, P. R. (eds), *Coccolithophores from Molecular Processes to Global Impact*. Springer, New York, pp. 481–508.

Bromowicz, J., 1986. Petrographic differentiation of source areas of Ropianka Beds east of Dunajec River (Outer Carpathians, Poland). *Annales Societatis Geologorum Poloniae,* 56: 253–276.

Brusatte, S. L., Butler, R. J., Barrett, P. M., Carrano, M. T., Evans, D. C., Lloyd, G. T., Mannion, P. D., Norell, M. A., Peppe, D. J., Upchurch, P. & Williamson, T. E., 2015. The extinction of the dinosaurs. *Biological Reviews,* 90: 628–642.

Burnett, J. A., 1998. Upper Cretaceous. In: Bown, P. R. (ed.), *Calcareous Nannofossils Biostratygraphy.* Cambridge University Press, Cambridge, pp. 132–199.

Bukry, D., 1973. Coccolith and silicoflagellate stratigraphy, Tasman Sea and southwestern Pacific Ocean, Deep Sea Drilling Project, Leg 21. *Initial Reports Deep Sea Drilling Project,* 21: 885–893.

Chiu, T.-C. & Broecker, W. S., 2008. Toward better paleocarbonate ion reconstructions: new insight regarding the $CaCO_3$ size index. *Paleoceanography,* 23: PA2216, doi:10.1029/2008PA001599.

Dameron, S. N., Leckie, R. M., Clark, K., MacLeod, K. G., Thomas, D. J. & Lees, J. A., 2017. Extinction, dissolution, and possible ocean acidification prior to the Cretaceous/Paleogene (K/Pg) boundary in the tropical Pacific. *Palaeogeography, Palaeoclimatology, Palaeoecology,* 485: 433–454.

Davis, Ch. C., Webb, C. O., Wurdack, K. J., Jaramillo, C. A. & Donoghue, M. J., 2005. Explosive radiation of Malpighiales supports a mid-Cretaceous origin of modern tropical rain forests. *American Naturalist,* 165: 36–65.

Davis, J. C., 1986. *Statistics and Data Analysis in Geology*. *3rd Edition*. John Wiley & Sons Inc., New York, pp. 461–646.

Donnadieu, Y., Pucéat, E., Moiroud, M., Guillocheau, F. & Deconinck, J.-F. F., 2016. A better-ventilated ocean triggered by Late Cretaceous changes in continental configuration. *Nature Communications,* 7: 10316.

Dubicka, Z. & Peryt, D., 2012. Latest Campanian and Maastrichtian palaeoenvironmental changes: Implications from an epicontinental sea (SE Poland and western Ukraine). *Cretaceous Research,* 37: 272–284.

Elorza, J. & García-Garmilla, F., 1998. Palaeoenvironmental implications and diagenesis of inoceramid shells (Bivalvia) in the mid-Maastrichtian beds of the Sopelana, Zumaya and Bidart sections (coast of the Bay of Biscay, Basque Country). *Palaeogeography, Palaeoclimatology, Palaeoecology,* 141: 303–328.

Erba, E., 2004. Calcareous nannofossils and Mesozoic oceanic anoxic events. *Marine Micropaleontology,* 52: 85–106.

Eshet, Y. & Almogi-Labin, A., 1996. Calcareous nannofossils as paleoproductivity indicators in Upper Cretaceous organic-rich sequences in Israel. *Marine Micropaleontology,* 29: 37–61.

Farris, J. A., 1969. On the cophenetic correlation coefficient. *Systematic Biology,* 18: 279–285.

Frank, T. D. & Arthur, M. A., 1999. Tectonic forcings of Maastrichtian ocean-climate evolution. *Paleoceanography*, 14: 103–117.

Gale, A. S., 2011. The Cretaceous world. In: Culver, S. J. & Rawson, P. F. (eds), *Biotic Response to Global Change. The Last 145 Million Years.* Cambridge University Press, Cambridge, pp. 4–19.

Gardin, S., 2002. Late Maastrichtian to early Danian calcareous nannofossils at Elles (Northwest Tunisia). A tale of one million years across the K-T boundary. *Palaeogeography, Palaeoclimatology, Palaeoecology,* 178: 211–231.

Gasiński, M. & Uchman, A., 2011. The Cretaceous-Paleogene boundary in turbiditic deposits identified to the bed: A case study from the Skole Nappe (Outer Carpathians, southern Poland). *Geologica Carpathica,* 62: 333–343.

Giraudeau, J., 1992. Distribution of recent nannofossils beneath the Benguela system: southwest African continental margin. *Marine Geology,* 108: 219–237.

Gómez-Alday, J. J., López, G. & Elorza, J., 2004. Evidence of climatic cooling at the Early/Late Maastrichtian boundary from inoceramid distribution and isotopes: Sopelana sections, Basque Country, Spain. *Cretaceous Research,* 25: 649–668.

Hallam, A. & Perch-Nielsen, K., 1990. The biotic record of events in the marine realm at the end of the Cretaceous: calcareous, siliceous and organic-walled microfossils and macroinvertebrates. *Tectonophysics,* 171: 347–357.

Hammer, Ø., Harper, D. A. T. & Paul, D. R., 2001. Past: paleontological statistic software package for education and data analysis. *Paleontologica Electronica,* 4: 1–9.

Hart, M. B., Feist, S. E., Håkansson, E., Heinberg, C., Price, G. D., Leng, M. J. & Watkinson, P., 2005. The Cretaceous–Palaeogene boundary succession at Stevns Klint, Denmark: foraminifers and stable isotope stratigraphy. *Palaeogeography, Palaeoclimatology, Palaeoecology,* 224: 6–26.

Hassenkam, T., Johnsson, A., Bechgaard, K. & Stipp, S. L. S., 2011. Tracking single coccolith dissolution with picogram resolution and implications for CO_2 sequestration and ocean acidification. *Proceedings of the National Academy of Sciences,* 108: 8571–8576.

Hay, W. W., 2008. Evolving ideas about the Cretaceous climate and ocean circulation. *Cretaceous Research,* 29: 725–753.

Hennebert, M., 2012. Hunting for the 405-kyr eccentricity cycle phase at the Cretaceous–Paleogene boundary in the Aïn Settara section (Kalaat Senan, central Tunisia). *Carnets de Geologie,* 5: 93–116.

Hennebert, M., 2014. The Cretaceous-Paleogene boundary and its 405-kyr eccentricity cycle phase: A new constraint on radiometric dating and astrochronology. *Carnets de Geologie,* 14: 173–189.

Henriksson, A. S., 1993. Biochronology of the terminal Cretaceous calcareous nannofossil Zone of *Micula prinsii*. *Cretaceous Research,* 14: 59–68.

Huber, B. T., MacLeod, K. G., Watkins, D. K. & Coffin, M. F., 2018. The rise and fall of the Cretaceous Hot Greenhouse climate. *Global and Planetary Change,* 167: 1–23.

Jugowiec-Nazarkiewicz, M., 2007. Calcareous nannoplankton from Upper Cretaceous pelagic facies of the Subsilesian Unit, Polish Outer Carpathians. *Biuletyn Państwowego Instytutu Geologicznego,* 426: 53–90. [In Polish, with English summary.]

Keller, G., 2005. Biotic effects of late Maastrichtian mantle plume volcanism: implications for impacts and mass extinctions. *Lithos,* 79: 317–341.

Keller, G., 2008. Cretaceous climate, volcanism, impacts, and biotic effects. *Cretaceous Research,* 29: 754–771.

Keller, G. & Abramovich, S., 2009. Lilliput effect in late Maastrichtian planktic foraminifera: Response to environmental stress. *Palaeogeography, Palaeoclimatology, Palaeoecology,* 284: 47—62.

Keller, G., Punekar, J. & Mateo, P., 2016. Upheavals during the Late Maastrichtian: Volcanism, climate and faunal events preceding the end-Cretaceous mass extinction. *Palaeogeography, Palaeoclimatology, Palaeoecology,* 441: 137–151.

Kędzierski, M., Gasiński, M. A. & Uchman, A., 2015. Last occurrence of *Abathomphalus mayaroensis* (Bolli) foraminiferid index of the Cretaceous–Paleogene boundary: the calcareous nannofossil proof. *Geologica Carpathica,* 66: 181–195.

Kędzierski, M. & Leszczyński, S., 2013. A paleoceanographic model for the Late Campanian–Early Maastrichtian sedimentation in the Polish Carpathian Flysch basin based on nannofossils. *Marine Micropaleontology,* 102: 34–50.

Kędzierski, M., Rodríguez-Tovar, F. J. & Uchman, A., 2011. Vertical displacement and taphonomic filtering of nannofossils by bioturbation in the Cretaceous–Palaeogene boundary section at Caravaca, SE Spain. *Lethaia,* 44: 321–328.

Kinkel, H., Baumann, K. H. & Cepek, M., 2000. Coccolithophores in the equatorial Atlantic Ocean: Response to seasonal and Late Quaternary surface water variability. *Marine Micropaleontology,* 39: 87–112.

Kotlarczyk, J., 1978. Stratigraphy of the Ropianka Formation or of Inoceramian Beds in the Skole Unit of the Flysch Carpathians. *Prace Geologiczne, Polska Akademia Nauk, Oddział w Krakowie, Komisja Nauk Geologicznych,* 108: 1–82. [In Polish, with English summary.]

Książkiewicz, M., 1956. Geology of the northern Carpathians. *Geologische Rundschau*, 45: 369–411.

Larina, E., Garb, M., Landman, N., Dastas, N., Thibault, N., Edwards, L., Phillips, G., Rovelli, R., Myers, C. & Naujokaityte, J., 2016. Upper Maastrichtian ammonite biostratigraphy of the Gulf Coastal Plain (Mississippi Embayment, southern USA). *Cretaceous Research,* 60: 128–151.

Larson, R. L., 1991. Latest pulse of Earth: Evidence for a mid-Cretaceous super-plume. *Geology,* 19: 547–550.

Less, J. A., 2002. Calcareous nannofossils biostratigraphy illustrates paleoclimate changes in The Late Cretaceous Indian Ocean. *Cretaceous Research,* 23: 537–634.

Lees, J. A., Bown, P. R. & Mattioli, E., 2005. Problems with proxies? Cautionary tales of calcareous nannofossil paleoenvironmental indicators. *Micropaleontology,* 51: 333– 343.

Lees, J. A., Bown, P. R., Young, J. R. & Riding, J. B., 2004. Evidence for annual records of phytoplankton productivity in the Kimmeridge Clay Formation coccolith stone bands (Upper Jurassic, Dorset, UK). *Marine Micropaleontology,* 52: 29–49.

Li, L. & Keller, G., 1998. Maastrichtian climate, productivity and faunal turnovers in planktic foraminifera in South Atlantic DSDP sites 525A and 21. *Marine Micropaleontology,* 33: 55–86.

Li, L. & Keller, G., 1999. Variability in Late Cretaceous climate and deep waters: Evidence from stable isotopes. *Marine Geology,* 161: 171–190.

Linnert, C., Engelke, J., Wilmsen, M. & Mutterlose, J., 2016. The impact of the Maastrichtian cooling on the marine nutrient regime – evidence from midlatitudinal calcareous nannofossils. *Paleoceanography,* 31: 694–714.

Linnert, C., Robinson, S. A., Lees, J. A., Bown, P. R., Pérez-Rodríguez, I., Petrizzo, M. R., Falzoni, F., Littler, K., Arz, J. A. & Russell, E. E., 2014. Evidence for global cooling in the Late Cretaceous. *Nature Communications,* 5: 4194.

Łapcik, P., 2018. Sedimentary processes and architecture of Upper Cretaceous deep-sea channel deposits: a case from the Skole Nappe, Polish Outer Carpathians. *Geologica Carpathica,* 69: 71–88.

Łapcik, P., Kowal-Kasprzyk, J. & Uchman, A., 2016. Deep-sea mass-flow sediments and their exotic blocks from the Ropianka Formation (Campanian–Paleocene) in the Skole Nappe: a case from the Wola Rafałowska section (SE Poland). *Geological Quarterly,* 60: 301–316.

MacLean, D. M., 1985. Deccan traps mantle degassing in the terminal Cretaceous marine extinctions. *Cretaceous Research,* 6: 235–239.

MacLeod, K. G., 1994. Bioturbation, inoceramid extinction, and mid-Maastrichtian ecological change. *Geology,* 22: 139–142.

MacLeod, K. G. & Huber, B., 1996. Reorganization of deep ocean circulation accompanying a Late Cretaceous extinction event. *Nature,* 380: 422–425.

MacLeod, K. G., Isaza Londoño, C., Martin, E. E., Jiménez Berrocoso, Á. & Basak, C., 2011. Changes in North Atlantic circulation at the end of the Cretaceous greenhouse interval. *Nature Geoscience,* 4: 779–782.

Marshall, C. R. & Ward, P. D., 1996. Sudden and gradual molluscan extinctions in the Latest Cretaceous of Western European Tethys. *Science,* 274: 1360–1363.

Masse, J. P., Philip, J. & Camoin, G., 1995. The Cretaceous Tethys. In: Nairn, A. E. M., Ricou, L. E., Vrielynck, B. & Dercourt, J. (eds), *The Tethys Ocean*. Springer, Boston, pp. 215–236.

Mateo, P., Keller, G., Punekar, J. & Spangenberg, J. E., 2017. Early to Late Maastrichtian environmental changes in the Indian Ocean compared with Tethys and South Atlantic. *Palaeogeography, Palaeoclimatology, Palaeoecology,* 478: 121–138.

Miall, A. D., 2014. Updating uniformitarianism: stratigraphy as just a set of 'frozen accidents'. *Geological Society, Special Publications,* 404: 11–36.

Molina, E., Alegret, L., Arenillas, I., Arz, J. A., Gallala, N., Hardenbol, J., Von Salis, K., Steurbaut, E., Vandenberghe, N. & Zaghbib-Turki, D., 2006. The global boundary stratotype section and point for the base of the Danian Stage (Paleocene, Paleogene, "Tertiary", Cenozoic) at El Kef, Tunisia – original definition and revision. *Episodes,* 29: 263–273.

Nimura, T., Ebisuzaki, T. & Maruyama, S., 2016. End-Cretaceous cooling and mass extinction driven by a dark cloud encounter. *Gondwana Research,* 37: 301–307.

Nordt, L., Atchley, S. & Dworkin, S., 2003. Terrestrial evidence for two greenhouse events in the latest Cretaceous. *GSA Today,* 13: 4–9.

Olsson, R. K., Wright, J. D. & Miller, K. G., 2001. Paleobiogeography of *Pseudotextularia elegans* during the latest Maastrichtian global warming event. *Journal of Foraminiferal Research,* 31: 275–282.

Pardo, A. & Keller, G., 2007. *Guembelitria* blooms-environmental catastrophes index. In: Sinha, D. K. (ed.), *Micropaleontology: Application in Stratigraphy and Paleoocenography*. Narosa, New Dehli, India, pp. 211–225.

Pardo, A. & Keller, G., 2008. Biotic effects of environmental catastrophes at the end of the Cretaceous and Early Tertiary: *Guembelitria* and *Heterohelix* Blooms. *Cretaceous Research,* 29: 1058–1073.

Pavlishina, P. & Wagreich, M., 2012. Biostratigraphy and paleoenvironments in a northwestern Tethyan Cenomanian–Turonian boundary section (Austria) based on palynology and calcareous nannofossils. *Cretaceous Research,* 38: 103–112.

Peralta-Medina, E. & Falcon-Lang, H. J., 2012. Cretaceous forest composition and productivity inferred from a global fossil wood database. *Geology,* 40: 219–222.

Perch-Nielsen, K., 1981. Les nannofossils calcaires à la limite Crétacé–Tertiary pres d'El Kef, Tunisie. *Cahiers de Micropaleontologie,* 3: 25–37.

Punekar, J., Keller, G., Khozyem, H. M. & Spangenberg, J., 2016. A multi-proxy approach to decode the end-Cretaceous mass extinction. *Palaeogeography, Palaeoclimatology, Palaeoecology,* 441: 116–136.

Rajchel, J., 1990. Lithostratigraphy of the Upper Paleocene and Eocene deposits in the Skole Unit. *Zeszyty Naukowe AGH, Geologia*, 48: 1–112. [In Polish, with English summary.]

Roth, P. H. & Bowdler, J. L., 1981. Middle Cretaceous calcareous nannoplankton biogeography and oceanography of the Atlantic and Indian oceans. *SEMP Special Publications,* 32: 517–546.

Sakamoto, M., Benton, M. J. & Venditti, C., 2016. Dinosaurs in decline tens of millions of years before their final extinction. *Proceedings of the National Academy of Sciences of the United States of America,* 113: 5036–5040.

Shannon, C. E. & Weaver, W., 1949. *The Mathematical Theory of Communication.* University of Illinois Press, Champaign, 144 pp.

Sheldon, E., Ineson, J. & Bown, P., 2010. Late Maastrichtian warming in the Boreal Realm: Calcareous nannofossil evidence from Denmark. *Palaeogeography, Palaeoclimatology, Palaeoecology,* 295: 55–75.

Sissingh, W., 1977. Biostratigraphy of Cretaceous calcareous nannoplankton. *Geologie en Mijnbouw,* 56: 37–65.

Sloan, R. E., Rigby, J. K., Jr., Van Valen, L. M. & Gabriel, D., 1986. Gradual dinosaur extinction and simultaneous ungulate radiation in the Hell Creek Formation. *Science,* 232: 629–633.

Sprain, C. J., Renne, P. R., Vanderkluysen, L., Pande, K., Self, S. & Mittal, T., 2019. The eruptive tempo of Deccan volcanism in relation to the Cretaceous–Paleogene boundary. *Science,* 363: 866–870.

Steinmetz, J. C., 1994. Sedimentation of coccolithophores. In: Winter, A. & Siesser, W. G. (eds), *Coccolithophores.* Cambridge University Press*,* Cambridge, pp. 179–197.

Tan, P. N., Steinbach, M. & Kumar, V., 2006. Cluster analysis: Basics concepts and algorithms. In: *Introduction to Data Mining.* Pearson Addison-Wesley, Boston, pp. 125–145.

Tantawy, A. A., Keller, G. & Pardo, A., 2009. Late Maastrichtian volcanism in the Indian Ocean: Effects on calcareous nannofossils and planktic foraminifera. *Palaeogeography, Palaeoclimatology, Palaeoecology,* 284: 63–87.

Thibault, N., Galbrun, B., Gardin, S., Minoletti, F. & Le Callonnec, L., 2016. The end-Cretaceous in the southwestern Tethys (Elles, Tunisia): orbital calibration of paleoenvironmental events before the mass extinction. *International Journal of Earth Sciences,* 105: 771–795.

Thibault, N. & Gardin, S., 2010. The calcareous nannofossil response to the end-Cretaceous warm event in the Tropical Pacific. *Palaeogeography, Palaeoclimatology, Palaeoecology,* 291: 239–252.

Thibault, N., Gardin, S. & Galbrun, B., 2010. Latitudinal migration of calcareous nannofossil Micula murus in the Maastrichtian: Implications for global climate change. *Geology,* 38: 203–206.

Thibault, N. & Husson, D., 2016. Climatic fluctuations and sea-surface water circulation patterns at the end of the Cretaceous era: Calcareous nannofossil evidence. *Palaeogeography, Palaeoclimatology, Palaeoecology,* 441: 152–164.

Thierstein, H. R., 1976. Mesozoic calcareous nannoplankton biostratigraphy of marine sediments. *Marine Micropaleontology,* 1: 325–362.

Thierstein, H. R., 1980. Selective dissolution of Late Cretaceous and Earliest Tertiary calcareous nannofossils: experimental evidence. *Cretaceous Research,* 2: 165–176.

Thierstein, H. R., 1981. Late Cretaceous nannoplancton and the change at the Cretaceous–Tertiary boundary. In: Warme, J. E., Douglas, R. G. & Winterer, E. L. (eds), *The Deep Drilling Project: a decade of progress. Society of Economic Paleontologists and Geologists, Special Publication,* 32: 355–394.

Voigt, S., Gale, A. S., Jung, C. & Jenkyns, H. C., 2012. Global correlation of Upper Campanian–Maastrichtian successions using carbon-isotope stratigraphy: development of a new Maastrichtian timescale. *Newsletters on Stratigraphy,* 45: 25–53.

Watkins, D. K., 1992. Upper Cretaceous nannofossils from leg 120, Kergulen Plateau, Southern Ocean. *Proceedings of the Ocean Drilling Program, Scientific Results,* 120: 343–370.

Watkins, D. K. & Self-Trail, J. N., 2005. Calcareous nannofossils evidence from the existence of the Gulf Stream during the late Maastrichtian. *Paleoceanography,* 20: 1–9.

Watkins, D. K., Wise, S. W., Jr., Pospichal, J. J. & Crux, J., 1996. Upper Cretaceous calcareous nannofossils biostratigraphy and paleooceanography of the Southern Ocean. In: Moguilevsky, A. & Whatley, R. (eds), *Microfossils and Oceanic Environments.* University of Wales, Aberystwyth, pp. 355–381.

Wdowiarz, S., 1949. Structure géologique des Karpates marginales au sud-est de Rzeszów. *Biuletyn Państwowego Instytutu Geologicznego,* 11: 1–51. [In Polish, with French summary.]

Wing, S. L. & Boucher, L. D., 1998. Ecological aspects of the Cretaceous flowering plant radiation. *Annual Review of Earth and Planetary Sciences,* 26: 379–421.

Winter, A., Reiss, Z. & Luz, B., 1979. Distribution of living coccolithophore assemblages in the Gulf of Elat ('Aqaba). *Marine Micropaleontology*, 4: 197–223.

Wise, S. W., Jr., 1983. Mesozoic and Cenozoic calcareous nannofossils recovered by Deep Sea Drilling Project Leg 71 in the Falkland Plateau region, southwest Atlantic Ocean. *Initial Reports Deep Sea Drilling Project,* 71: 481–550.

Young, J. R., 1994. Function of Coccoliths. In: Winter, A. & Siesser, W. G. (eds), *Coccolithophores*. Cambridge University Press, Cambridge, pp. 63–82.

Ziveri, P., Thunell, R. C. & Rio, D., 1995. Export production of coccolithophores in an upwelling region: results from San Pedro Basin, Southern California Borderlands. *Marine Micropaleontology,* 24: 335–358.